X-ray absorption near-edge structure of GaN with high Mn concentration grown on SiC

2009 J. Phys.: Condens. Matter 21 295801

(http://iopscience.iop.org/0953-8984/21/29/295801)

J. Phys.: Condens. Matter **21** (2009) 295801 (8pp) doi:10.1088/0953-8984/21/29/295801

X-ray absorption near-edge structure of GaN with high Mn concentration grown on SiC

O Sancho-Juan[1], A Cantarero[1], N Garro[1], A Cros[1], G Martínez-Criado[2], M Salomé[2], J Susini[2], D Olguín[3] and S Dhar[4,5]

[1] Materials Science Institute, University of Valencia, PO Box 22085, E46071 Valencia, Spain
[2] European Synchrotron Radiation Facility, 6 rue Jules Horowitz, 38043 Grenoble, France
[3] Dept. de Física, CINVESTAV—IPN, 07300 México D F, Mexico
[4] Experimentalphysik, Universität Duisburg-Essen, Lotharstraße 1, 47057 Duisburg, Germany
[5] Paul Drude Institute, Hausvogteiplatz 5-7, 10117 Berlin, Germany

Received 24 November 2008, in final form 18 March 2009
Published 3 July 2009
Online at stacks.iop.org/JPhysCM/21/295801

Abstract

By means of x-ray absorption near-edge structure (XANES) several $Ga_{1-x}Mn_xN$ ($0.03 < x < 0.09$) layers have been analyzed. The Mn-doped GaN samples consisted of different epilayers grown by molecular beam epitaxy on [0001] SiC substrates. The low mismatch between GaN and SiC allows for a good quality and homogeneity of the material. The measurements were performed in fluorescence mode around both the Ga and Mn K edges. All samples studied present a similar Mn ionization state, very close to 2+, and tetrahedral coordination. In order to interpret the near-edge structure, we have performed *ab initio* calculations using the full potential linear augmented plane wave method as implemented in the Wien2k code. The calculations show the appearance of a Mn bonding $t_2 \uparrow$ band localized in the gap region, and the corresponding anti-bonding state $t_2 \downarrow$, which seem to be responsible for the double structure which appears at the pre-edge absorption region. The shoulders and main absorption peak of the XANES spectra are attributed to transitions from the Mn(1s) band to the conduction bands, which are partially dipole allowed because of the Mn(4p) contribution to these bands.

(Some figures in this article are in colour only in the electronic version)

1. Introduction

Since the discovery of ferromagnetism (FM) in Mn-doped GaAs [1], a large amount of work has been devoted to the growth and characterization of diluted magnetic semiconductors (DMSs) [2]. The ideal DMS is a semiconductor material doped with a ferromagnetic impurity, presenting FM above room temperature and, additionally, free carriers to allow spin injection in a non-FM material, necessary in the implementation of a commercial device. Among the III–V compounds, Mn-doped GaP seems to be the zinc-blende semiconductor with the highest Curie temperature (T_C) and Mn- or Cr-doped GaN the highest T_C FM semiconductor material [3, 4]. Recently, a high $T_C = 700$ K has been measured in Cu-doped GaP [5]. The highest T_C measured in Mn-doped GaN is 940 K [6, 7]. A recent review pays particular attention to III–V DMS materials doped with Mn [8].

From the experimental point of view, besides the works of Hori and collaborators [6, 7, 9, 10], many works on the magnetic properties of Mn-doped GaN show significantly different results. So far, most of the produced materials are grown on Al_2O_3 substrates, and present Mn micrometric clusters considered frequently as the origin of the FM [11–13]. Moreover, in highly doped samples, the zinc-blende and wurtzite polytypes of GaN often coexist [14]. In other DMSs like GaMnAs, Mn has been found to be interstitial in samples with high Mn content [15], a possible source of phase mixture. Manganese has been found to be also in interstitial location when grown on Si [16], but it is more common to find it in substitution for the Ga, at least in the wurtzite structure [17, 14]. A set of theoretical works in Mn-doped GaN, on the other hand, based on either microscopic theories [18] or *ab initio* calculations [19], claims the existence of FM above room temperature. In a recent work, Kang

et al [20] found out that $Ga_{1-x}Mn_xN$ is ferromagnetic above room temperature for $x > 0.06$. They have also found that, when the Mn concentration increases, the formation of small Mn metallic clusters is energetically favorable, which can also contribute to the FM.

Clearly, for a better understanding of the FM in Mn-doped GaN it is necessary to improve the crystal quality of the material and the homogeneity in the distribution of Mn. In this direction, SiC presents a very important advantage over sapphire or silicon as a substrate: its lattice mismatch with GaN is only 3.5%. Therefore, the strain state of GaN films grown on SiC is much smaller than that deposited on other materials (the lattice mismatch is around 13% for GaN on the (0001) Al_2O_3 plane). In this work, we have studied different $Ga_{1-x}Mn_xN$ epilayers with Mn content up to ∼9% grown by molecular beam epitaxy (MBE) on 4H- and 6H-SiC(0001) substrates. In a previous study [21], the existence of nanometric clusters (2–5 nm) of unknown origin was shown by transmission electron microscopy in the sample with the highest Mn content, which presents FM with a $T_C \sim 750$ K. Details of the sample growth, as well as preliminary x-ray absorption related results, can be found elsewhere [21, 22].

In the present work we analyze the local arrangement of Mn in the GaN host lattice and a possible mixture of phases, particularly in the sample with the highest Mn concentration. Moreover, we will study the possible formation of punctual or extended defects (e.g. residual impurities and precipitates) in the host GaN, since they may also be present and could play an important role in the distribution of the Mn element and its magnetic order. Finally, to determine the valence state of Mn and its possible variation with the manganese content x, and to clarify the microscopic picture of FM, the electronic structure has been analyzed in detail by x-ray absorption near-edge structure (XANES) spectroscopy.

2. Experimental set-up

X-ray fluorescence and XANES measurements were carried out at the micrometer scale in the soft and hard x-ray beamlines (ID21 and ID22) of the European Synchrotron Radiation Facility. Both microprobes, operating in complementary energy ranges, are equipped with insertion device sources, Si mirrors for harmonic rejection, and fixed-exit double Si(111) crystal monochromators ($\Delta E/E \approx 10^{-4}$). At ID21, the monochromatic beam is focused on the sample surface up to 500 nm beam size using chromatic Au Fresnel zone plates (photon flux $\approx 10^9$ photons s^{-1} at the Mn K edge). At ID22, the spatial resolution of 1.5×3.5 μm^2 is reached by achromatic Kirkpatrick–Baez Si mirrors (photon flux $\approx 10^{11}$ photons s^{-1} at the Ga K edge). The intensity of the incident x-ray beam at ID21 is detected with a Si diode associated with a fluorescence foil, whereas at ID22 an ionization chamber filled adequately with a gas mixture monitors the photon flux. Finally, single element solid state detectors with Si(Li) and Ge crystals are used to collect the characteristic x-ray fluorescence lines at ID22 and ID21, respectively.

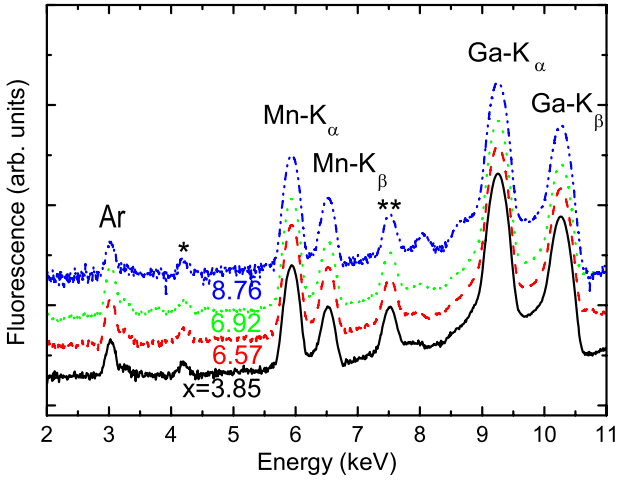

Figure 1. X-ray fluorescence spectra, in logarithmic scale, of $Ga_{1-x}Mn_xN$/SiC samples with different Mn contents measured at 45° geometry at an excitation energy of 12 keV. The spectra have been rescaled to have the same intensity at the Ga Kα peak, and have been shifted for clarity. The solid line (black online) corresponds to a Mn concentration of 3.85%, the dashed line (red online) to 6.57%, the dotted line (green online) to 6.92%, and the dashed–dotted line (blue online) to 8.76%. The main peaks observed are the Mn and Ga Kα and Kβ emissions and the fluorescence peak of Ar around 3 keV. The peak labeled with a star is the 1.74 keV escape peak of Mn and the one with two stars the 1.74 keV escape peak of Ga.

3. Experimental results

3.1. X-ray fluorescence

The average x-ray fluorescence spectra of the GaN layers with different Mn contents, measured at ID22, are shown in figure 1, taken at 11 keV over a 50×50 μm^2 scanned area. All the spectra were recorded with an incident angle of $\theta = (45 \pm 1)°$ with respect to the sample surface. The Kα and Kβ fluorescence lines of Mn and Ga atoms, as well as the Ar signal from the air, are represented. The escape peaks generated from the solid state detector at 1.74 keV (Si Kα energy) from the Ga and Mn parent lines are also indicated. The information depth of the fluorescence photons is about 4.6 and 7.1 μm at the Mn and Ga Kα photon energies, respectively, for an excitation energy of 12 keV. Within the experimental accuracy, no additional background impurities were detected in the considered energy range. By setting the several energy regions of interest around the dominant fluorescence lines, and taking advantage of the XYZ piezo-scanning capabilities at both microscopes, the compositional homogeneity of all samples was analyzed. Ranging from 3.85% up to about 8.76%, the Mn concentrations were estimated from the Mn and Ga Kα line intensity ratio (see table 1 in section 5.2) [23]. In the calculations, we have used $\rho = 6.15$ g cm^{-3} for the GaN density and $d \approx 0.5 \pm 0.1$ μm for the layer thickness.

Figure 2 shows the elemental maps of Ga and Mn for the sample with 8.76% of Mn content. They have been obtained by mapping the fluorescence of a region of 50×50 μm^2 and integrating around the Ga Kα and Mn Kα peaks, once the background had been removed. The scales indicate, in arbitrary units, the variation of Mn (left panel) or Ga (right

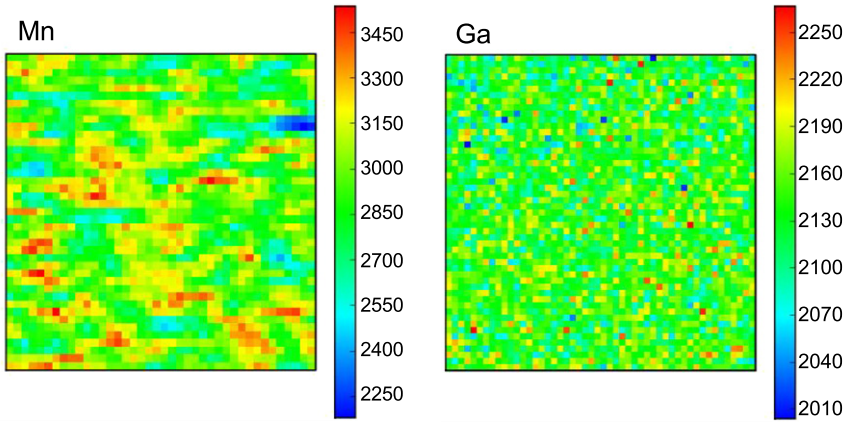

Figure 2. X-ray fluorescence maps of the sample with 8.76% of Mn content in an area of 50 × 50 μm^2, measured in the same conditions as explained in the caption of figure 1. The left panel shows the distribution of Mn while the right panel the Ga distribution. The scales are in arbitrary units.

Table 1. Parameters obtained from the Gaussian fits of the pre-edge regions. x is the Mn content, A_1 and A_2 the peak position, and γ_1, γ_2, S_1 and S_2 the corresponding broadenings and areas (intensity).

x (%)	A_1 (eV)	γ_1 (eV)	S_1	A_2 (eV)	γ_2 (eV)	S_2
3.85	6539	1.14(11)	0.180	6541	2.14(8)	0.820
6.92	6539	1.15(13)	0.130	6541	2.15(9)	0.870
8.76	6539	3(6)	0.087	6541	2.5(5)	0.910

panel) across the mapped surface. The spatial variation of Mn in the mapped region is a few per cent. There is a small region on the right with a very low Mn content, which we attribute to the holes produced by sample cleaning [21, 24]. The Ga concentration also decreases in this region. The right panel shows the variation of the Ga concentration in the same region. We can observe how the Ga content is nearly constant, if we neglect individual pixels with a larger or lower Ga content which do not correspond to Mn variation and must be attributed to statistical factors.

3.2. X-ray absorption near-edge spectroscopy

Figure 3 shows the Mn K-edge XANES data recorded in fluorescence detection mode at ID21. The measurement conditions included a photon energy range of 6496–6682 eV, an energy step of 0.5 eV, and integration times determined by the counting statistics. The spectra have been normalized to the incident photon intensity and, after subtraction of the pre-edge background, have been scaled to the maximum peak height. In spite of the small variation of the Mn content found in the fluorescence maps, the XANES spectra collected at different sample locations are similar. Above the edge, there is almost no spectral change as a function of the Mn content, suggesting insignificant doping-induced disorder in the host compound. Except the small differences in the pre-edge regions analyzed later, the XANES data have identical spectral features, revealing independent partial density of unoccupied Mn p states in the conduction band with the Mn content. A comparison with the XANES spectra taken around the Ga K-edge [22] displays similar results: there

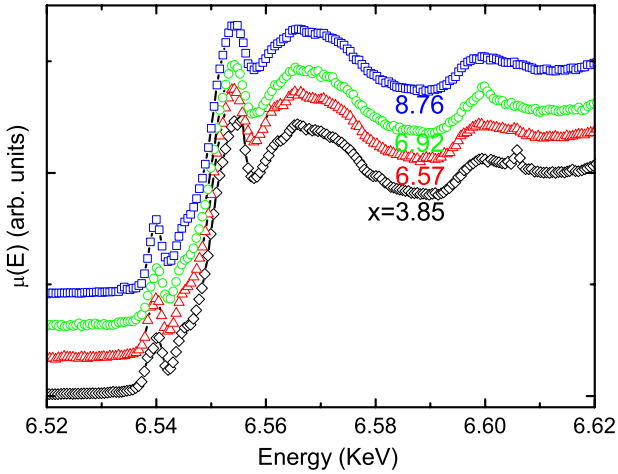

Figure 3. Room temperature x-ray absorption spectra of the GaN:Mn/SiC samples measured in 45° geometry around the Mn K edge. The spectra have been rescaled to have the same intensity far from the edge, and shifted for clarity. The rhombi (black online) correspond to a Mn content of 3.85%, the up triangles (red online) to 6.57%, the circles (green online) to 6.92%, and the squares (blue online) to 8.76%.

is a close correspondence among the respective oscillations at all Mn levels. Therefore, in contrast to the GaMnAs system [15], where the Mn atoms frequently occupy interstitial positions at high concentrations, the similarity between the XANES spectra measured at the Mn or Ga K edges [22] strongly suggests a substitutional incorporation of the Mn in GaN when grown on SiC, even for highly doped samples. The polarization-dependent XANES measurements, used to elucidate a possible mixing of zinc-blende and wurtzite phases [25], also supported the retention of the hexagonal order, showing the expected anisotropic effects for all Mn concentrations.

3.3. Valence state of Mn

To study the edge region and consequently the valence state in our samples, the normalized XANES spectra for different

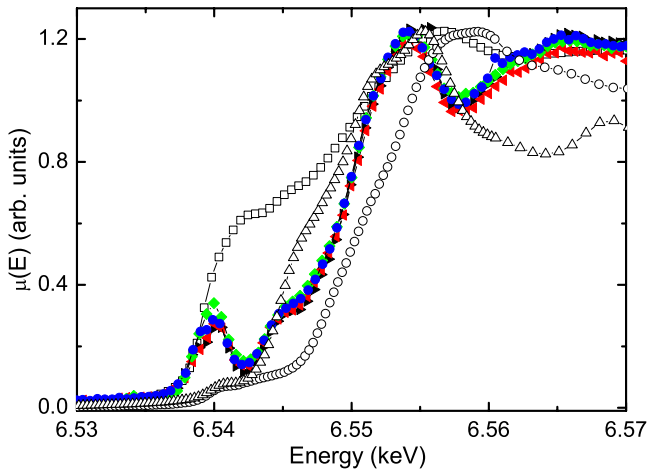

Figure 4. XANES spectra of the GaN:Mn/SiC samples measured in 45° geometry around the Mn K edge. The full right triangles (black online) correspond to a Mn content of 3.85%, the full left triangles (red online) to 6.57%, the full rhombi (green online) to 6.92%, and the full circles (blue online) to 8.76%. For a direct comparison, the absorption spectra of several model compounds are also shown: metallic Mn (open squares), MnO (open up triangles) and Mn_2O_3 (open circles). The corresponding valence states of these compounds are 1+, 2+ and 3+, respectively. The spectra of our samples are rescaled to have the same intensity far from the edge. The model compounds have been rescaled to their maximum value.

Mn compounds (metallic Mn, MnO and Mn_2O_3) are shown in figure 4. The MnO (Mn^{2+}) has the edge at 6550.3 eV, while that of Mn_2O_3 (Mn^{3+}) is located at 6553.8 eV. From the direct comparison, we deduce that most of the Mn atoms have an ionization state between 2+ and 3+. This point will be analyzed more carefully in section 5. Although model compounds with local structures similar to the wurtzite GaN crystal lattice are the ideal situation, only Mn oxides were available as references. Therefore, the comparison above reveals clear differences from all the XANES data and suggests predominant tetrahedral coordination of Mn atoms in $Ga_{1-x}Mn_xN$ on SiC.

4. *Ab initio* calculations

To determine the origin of the pre-edge peaks and the effect of Mn on the electronic properties of GaN, we have performed an *ab initio* calculation of the GaN wurtzite structure, incorporating the Mn impurity. The study uses the full potential linear augmented plane wave method as implemented by Blaha *et al* in the Wien2k code [26]. The program, within the density functional formalism, uses the generalized gradient approximation to compute the exchange–correlation part of the energy and supplies accurate electronic band structures. Careful attention was paid to assure the convergence of the total energy in terms of the variational cut-off-energy parameter, where a value of 10 Ryd was used. At the same time, we have used an appropriate set of k-points to compute the total energy. A total of 50 k-points in the irreducible sector of the Brillouin zone (BZ) were used. This choice is equivalent to a $5 \times 5 \times 6$ Monkhorst–Pack [27] grid of the unit cell.

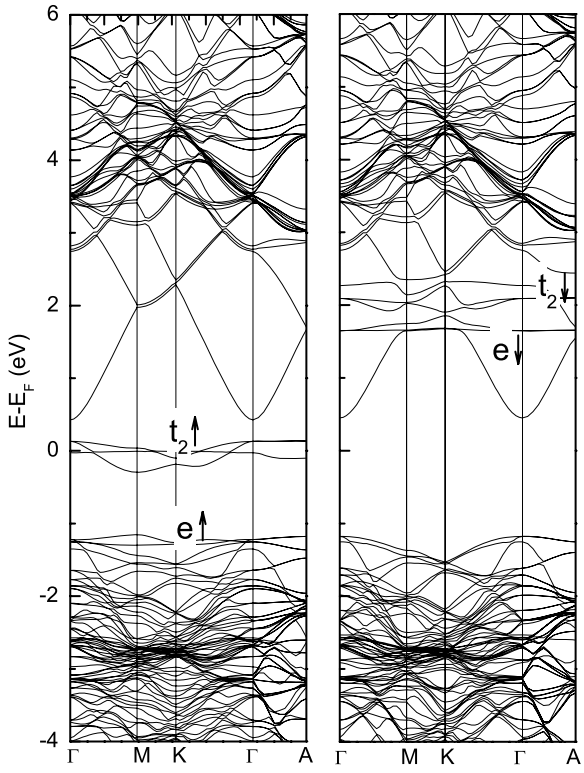

Figure 5. Band structure of $Ga_{35}MnN_{36}$ corresponding to a $3 \times 3 \times 2$ supercell, calculated with the Wien code as explained in the text. The left panel refers to the spin up component and the right one to spin down. The t_2 and e states of the Mn are explicitly indicated.

To simulate the incorporation of Mn, we have constructed a supercell consisting of $2 \times 2 \times 1$ GaN cells (one Mn atom per supercell, which is equivalent to 12.5% Mn) or $3 \times 3 \times 2$ GaN cells (one Mn atom per supercell, equivalent to 2.8% Mn). The Mn atom was taken at the center of the cell and the atomic positions of the different species were optimized in both supercells.

Figure 5 shows the calculations of the band structure for the supercell corresponding to 2.8% of Mn ($Ga_{35}MnN_{36}$). The smaller calculated supercell gives similar results, although with a slightly different energy of the Mn d levels. The left panel of figure 4 corresponds to spin up and the right panel to spin down. Since the number of atoms in the supercell is 18 times larger than in the GaN unit cell, the number of bands must be multiplied by 18 or, in other words, the BZ has been folded into a mini-BZ 18 times smaller. In spite of the number of bands, we can clearly identify the $e\uparrow$ states of the Mn at the top of the GaN valence band. The $t_2\uparrow$ bonding state of Mn, on the other hand, is located in the region of the forbidden band. In the right panel we can observe the corresponding anti-bonding states ($e\downarrow$ and $t_2\downarrow$) shifted up in energy within the conduction band.

5. Discussion

As we have already commented in the previous section, two important results can be stated: first, the Mn atoms are found

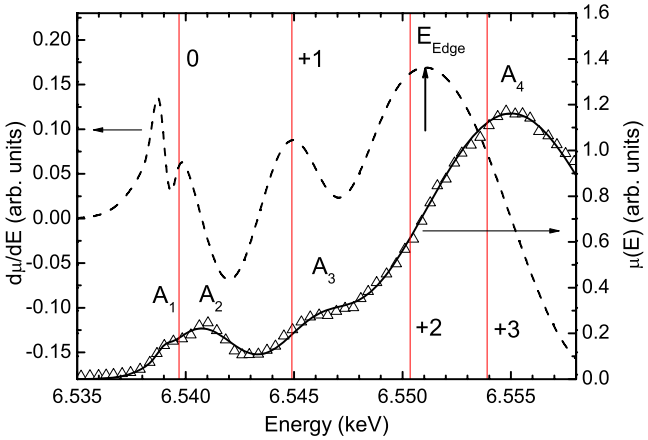

Figure 6. XANES spectrum of the 3.8% Mn content GaN:Mn/SiC sample (open up triangles) and the corresponding multi-Gaussian fit (solid line), as explained in the text. The first energy derivative of the Gaussian fit, depicted with a dashed line, indicates the position of the maxima of the slopes, indicating the edge energy. The different Mn oxidation states derived from the standard compounds are indicated by vertical straight lines.

to be substitutional for Ga in the samples analyzed here, independently of the Mn content. Second, the Mn distribution is random, as has been established by the mapping analysis. There are, however, a couple of important points which must be analyzed: (i) what is the valence of Mn in our samples, and (ii) what is the physical origin of the pre-edge structure and why the pre-edge profile changes with increasing Mn content. These points will be clarified in this section.

5.1. Valence state of Mn

As already observed in figure 3, the XANES spectra of all samples present a complicated pre-edge structure. In order to determine more precisely the valence state of Mn in our samples, we have proceeded in the following way. First, we have fitted the pre-edge and edge structure with four Gaussians, as shown in figure 6, to account for the main structures observed. The peak positions of the Gaussians are labeled A_1, A_2, A_3, and A_4. Since the valence is determined from the edge position, we have drawn the derivative of the Gaussian fit (dotted curve in the figure) to find it. The position of the different maxima corresponds to the region where the slope presents a maximum. Clearly, the upper maximum around 6551 eV corresponds to the edge energy. We have indicated in the figure, on the other hand, by means of vertical lines, the position of the edge for different valence states, obtained from the derivatives of the Mn compounds. In this way we can state more accurately that the valence of the Mn in the sample with 3.8% Mn is around 2.2+. By using the same procedure, we can determine the edge position of the other samples, being in the same region within experimental uncertainties. As mentioned before, in the samples studied by Sonoda *et al* [10, 6] Mn also has a valence around 2+. Most of the samples studied in the literature, however, present valence 3+ or even 3.3+ [11].

5.2. Physical origin of the pre-edge region

If we pay attention to the pre-edge region of the different samples, we can realize that the relative intensity of the first two peaks (A_1 and A_2) is different depending on the doping concentration. In the sample with lower Mn content the two peaks are clearly visible, while in the sample with the highest Mn concentration we hardly observe peak A_1.

To analyze the evolution of the relative intensity of A_1 and A_2, we show in figure 7 the double-peak structure A_1–A_2 measured in the samples with 3.85 (left panel), 6.92 (center panel) and 8.76% Mn (right panel) content. The sample with 6.57% Mn shows a similar result as compared to that shown in the central panel. The double-peak structure has been fitted with the help of two Gaussians, where we have kept the peak position as constant. This can be justified since these two peaks originate from two different electronic transitions of specific energy. Table 1 shows the parameters obtained from the fitting of three of the samples, which are basically the peak position (labeled as A_1 and A_2), the peak broadening γ_1 and γ_2 and the corresponding areas S_1 and S_2. From the results shown in the table, we can extract the following information: (i) the positions of peaks A_1 and A_2 can be kept constant for all Mn concentrations; (ii) the broadenings of the peaks are of the same order and do not show a correlation with the Mn content (in the sample with more Mn there is an increase in the broadening, but at the same time the uncertainty is much larger); (iii) the relative area or intensity of the peaks ($S_1+S_2 = 1$) changes significantly with the Mn content. There is a systematic variation of the intensity of the A_1 peak with the Mn content.

To clarify the origin of this variation, we need to identify the transitions corresponding to peaks A_1 and A_2. We have performed a XANES calculation with the Wien2k program, with the structure corresponding to the $Ga_{35}MnN_{36}$ supercell. The result of the calculation is shown in figure 8 (left panel), where we have added the label A_{34} to the small structure (shoulder) between A_3 and A_4. The experimental data, corresponding to the sample with 3.85% Mn, are given by open circles, while the solid line refers to the XANES spectra; the dashed and dotted line are the spin up and spin down contributions, respectively. The main features observed in the experiment are reproduced by the theory. The energy shift of the transitions is originated by the well known gap problem of *ab initio* calculations. The energy scale is referred to the Fermi level, which separates full from empty electronic states. The A_1 peak is located at the Fermi level. For simplicity, i.e. to elude the mesh formed with the band folding in the supercell, we have drawn the band structure of pure GaN in the right panel of figure 8, and incorporated the important Mn levels with horizontal shadow regions, as localized band states. The horizontal line at the bottom corresponds to the Mn(1s) band, which is flat (and narrow), since the states are completely localized. The transitions observed in an absorption experiment are vertical, because of wavevector conservation, but their origin can be any point of the BZ. From energy considerations and looking at the partial density of p states of Mn, the different transitions can be assigned. The transition to A_4 is very intense due to the large density of states,

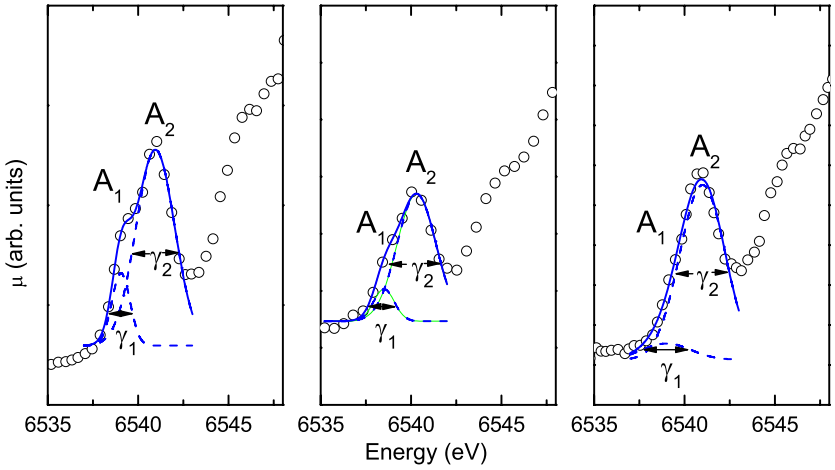

Figure 7. Normalized XANES spectra around the pre-edge of the Mn K edge for three of the samples studied. From the left to the right panel, the spectra correspond to 3.85, 6.92, and 8.76% Mn content, respectively. The solid lines are the corresponding multi-Gaussian fits (areas S_1 and S_2 and full widths at half maximum γ_1 and γ_2), corresponding to peaks A_1 and A_2, respectively.

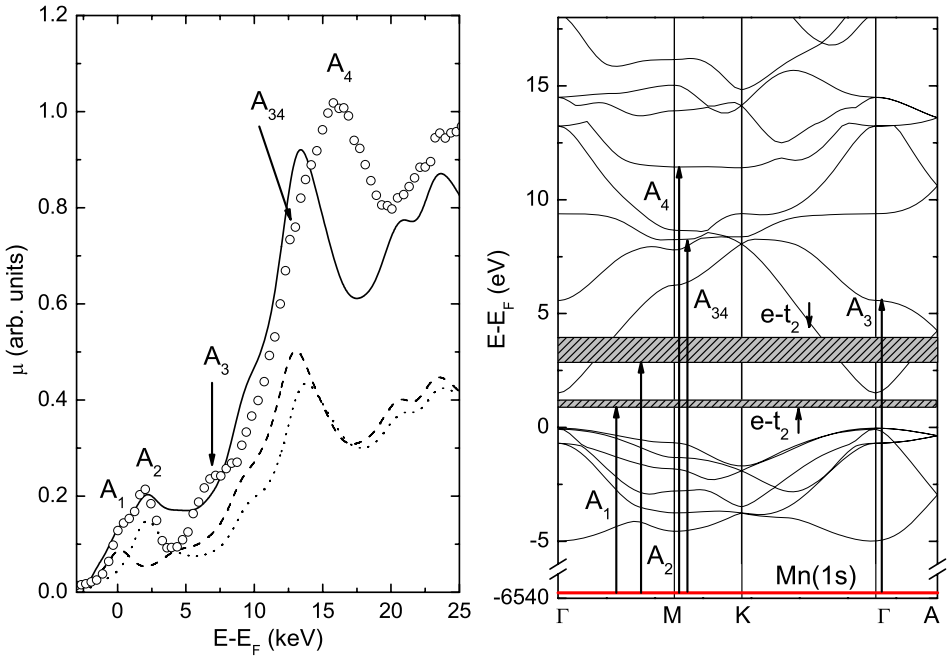

Figure 8. Left panel: comparison between the calculated partial DOS and the XANES spectrum for the 3.8% Mn concentration. Points are the experimental data while the solid line is the theoretical XANES spectrum (for $Ga_{35}MnN_{36}$, corresponding to ∼2.8% Mn). The dashed and dotted lines correspond to the contribution of the transition to $t_2\uparrow$ and $t_2\downarrow$, respectively. Right panel: band structure of GaN, calculated using the WIEN code as explained in the text. The localized band d states of Mn have been drawn in a schematic way. The transitions measured in the XANES spectra shown in the left panel are indicated in the band structure with up arrows in the figure, and labeled correspondingly.

given by the flatness of the upper band. It is important to point out that all transitions (A_1 to A_4 and upper transitions) are possible because of the mixing of the conduction band states of GaN with the p states of Mn (from selection rules, there must be a change in the band parity for a transition to be dipole allowed).

Let us remember the origin of the localized states of Mn. The isolated Mn atom has the electronic configuration $[Ar]3d^54s^2$. If the valence of the Mn is 2+ the configuration is $[Ar]3d^5$, while for a 3+ valence the electronic configuration is $[Ar]3d^4$. From the XANES spectra (figure 3) we deduced that Mn is in a tetrahedral configuration. In that case, the d levels of Mn in a solid are split into e (with two electrons) and t_2 (with three electrons), e being the lowest energy level. There are, actually, bonding (valence band) and anti-bonding (conduction band) states. If the valence of Mn is 3+ ($[Ar]3d^4$) the $e + t_2$ bonding states are partially filled, while if the Mn is in 2+ configuration ($[Ar]3d^5$) the $e + t_2$ bonding states are occupied. In the last case, the first unoccupied level is the $e+t_2$ anti-bonding states in the conduction band and we can observe only one peak (A_1) in the XANES spectra (the resolution is not enough to see the $e - t_2$ splitting). In the case of a lower

valence of Mn, the bonding states are partially occupied and the XANES spectra show two peaks, A_1 and A_2, corresponding to $e + t_2 \uparrow$ and $e + t_2 \downarrow$.

In the theoretical band structure (right panel of figure 8) the position of the Fermi level indicates that the $e \uparrow$ states are occupied, while the $t_2 \uparrow$ states have only two-thirds of the possible occupation. Since Mn is substituting a Ga (which contributes with three electrons to the bond), and the Mn contributes with six electrons ($4s^2 3d^5$), the theoretical calculations give a valence 3+ to the Mn. We need one more electron to arrive at a Mn d^5 configuration, in which the Mn would have the maximum magnetic moment. Since the peak A_2 has five empty states, these states will be filled in with x-ray photons and will be more intense than A_1 (which have only one empty state). This is basically right when compared with the experiment. Actually, in the sample with lower Mn concentration we observe two peaks, the intensity of the first peak being smaller than the one of the second peak, in agreement with theory. But, as soon as we increase the Mn content, the intensity of peak A_1 goes to zero, in contrast with the electronic band calculations. The only possible reason is that the population of the $t_2 \uparrow$ band increases with increasing Mn concentration, and in the sample with the largest Mn content this band is practically occupied: then, the transition with lower energy can only take place from the Mn(1s) band to the anti-bonding bands $(e - t_2) \downarrow$ (peak A_2), since the bounding states are occupied. This is in agreement with the fact that the peak A_1 has been observed by other authors with a larger intensity, the valence of the Mn being 3+ or 3.3+ in their samples [11]. The results are also in agreement with the calculations of Farges [28], who analyzed the pre-K-edge region of oxide-type materials with Mn: in the case of tetrahedral coordination, the compounds with Mn^{2+} present a single peak in the pre-edge region, while there is a double peak in compounds with Mn^{3+}.

The only open question now is where the extra electrons come from. A possible explanation to this answer comes from the fact that GaN is grown by plasma-enhanced molecular beam epitaxy. The quantity of hydrogen in the samples could increase with the Mn content. In the samples grown by Sonoda *et al* [6], they also have valence close to 2+ and grow by a similar technique. Another option is the existence of many nitrogen vacancies. Yang *et al* [29] have found a tremendous increase in the number of nitrogen vacancies correlated to the Mn content in GaN. To know the real origin of the additional electrons requires additional effort, possibly with the use of optical techniques.

6. Conclusions

We have analyzed the XANES spectra of a set of Mn-doped (Mn content from 3.85 to 8.76%) GaN samples grown by plasma-enhanced molecular beam epitaxy on SiC. We show that the samples have the wurtzite structure and that Mn substitutes Ga for all concentrations studied. The samples present a homogeneous distribution of Ga independently of the Mn concentration. The XANES spectra show a pre-edge region, a fingerprint of the Mn coordination. We have performed an *ab initio* calculation of GaN and a $Ga_{35}MnN_{36}$ supercell to interpret the physical origin of the pre-edge and relative intensity of the peaks conforming the structure. These calculations have allowed us to obtain the XANES spectrum and compare it with the experimental data. We concluded that the first x-ray absorption transition (A_1) takes place from the Mn(1s) band to the $e - t_2 \uparrow$ band, partially occupied. The occupation of this band increases with increasing Mn content and peak A_1 disappears.

No clear explanation is found for the valence of Mn in our samples, although the excess of hydrogen originating from the growth method could be responsible for the disappearance of the A_1 transition in the sample with larger Mn content. The valence of 2+ found in the sample with higher Mn content could be the origin of the stronger FM in that sample.

Acknowledgments

This work has been partially supported by the Ministerio de Educación y Ciencia of Spain (grant MAT2006-1825), and the European Synchrotron Radiation Facility.

References

[1] Ohno H, Shen A, Matsukara F, Oiwa A, Endo A, Katsumoto S and Iye Y 1996 *Appl. Phys. Lett.* **69** 363
[2] Liu C, Yun F and Morkoç H 2005 *J. Mater. Sci.* **16** 555–97
[3] Dietl T, Ohno H, Matsukura F, Cibert J and Ferrand D 2000 *Science* **287** 1019
[4] Pearson S J *et al* 2004 *J. Phys.: Condens. Matter* **16** R209
[5] Gupta A, Owens F J, Rao K V, Iqbal Z, Guille J M O and Ahuja R 2006 *Phys. Rev.* B **74** 224449
[6] Hori H, Sonoda S, Sasaki T, Yamamoto Y, Shimizu S, Suga K and Kindo K 2002 *Physica* B **324** 142
[7] Sonoda S *et al* 2006 *J. Phys.: Condens. Matter* **18** 4615–21
[8] Burch K S, Awschalom D D and Basov D N 2008 *J. Magn. Magn. Mater.* **320** 3207–28
[9] Yoshii S, Sonoda S, Yamamoto T, Kashiwagi T, Hagiwara M, Yamamoto Y, Akasaka Y, Kindo K and Hori H 2007 *Eur. Phys. Lett.* **78** 37006
[10] Sonoda S *et al* 2007 *Appl. Phys. Lett.* **90** 012504
[11] Giraud R, Kuroda S, Marcet S, Bellet-Amalric E, Biquard X, Barbara B, Fruchart D, Ferrand D, Cibert J and Mariette H 2004 *Europhys. Lett.* **65** 553
[12] Martínez-Criado G, Somogyi A, Hermann M, Eickhoff M and Stutzmann M 2004 *Japan. J. Appl. Phys.* **43** L695
[13] Kim N, Lee S J and Kang T W 2004 *Phys. Lett.* A **329** 226
[14] Martínez-Criado G, Somogyi A, Ramos S, Campo J, Tucoulou R, Salomé M, Susini J, Hermann M, Eickhoff M and Stutzmann M 2005 *Appl. Phys. Lett.* **86** 1–3
[15] Yu K M, Walukiewicz W, Wojtowicz T, Kuryliszyn I, Liu X, Sasaki Y and Furdyna J K 2002 *Phys. Rev.* B **65** 201303
[16] Niermann T, Mai D, Roever M, Kocan M, Zenneck J, Malindretos J, Rizzi A and Seibt M 2008 *J. Appl. Phys.* **103** 073520
[17] Titov A *et al* 2005 *Phys. Rev.* B **72** 115209
[18] Krstajić P M, Peeters F M, Ivanov V A, Kurnakov N S, Fleurov V and Kikoin K 2004 *Phys. Rev.* B **70** 195215
[19] Sato K, Hederichs P H, Katayama-Yoshida H and Kudronovsky J 2004 *J. Phys.: Condens. Matter* **16** S5491–7
[20] Kang J, Chang K J and Katayama-Yoshida H 2005 *J. Supercond.* **18** 55–60
[21] Dhar S, Brandt O, Trampert A, Däweritz L, Friedland K J, Ploog K H, Keller J, Beschoten B and Güntherodt G 2003 *Appl. Phys. Lett.* **82** 2077–9

[22] Sancho-Juan O, Cantarero A, Martinez-Criado G, Olguin D, Garro N, Cros A, Salome M, Susini J, Dhar S and Ploog K 2006 *Phys. Status Solidi* b **243** 1692
[23] Somogyi A, Martínez-Criado G, Homs A, Hernandez-Fenollosa M A, Vantelon D and Ambacher O 2007 *Appl. Phys. Lett.* **90** 181129
[24] Sancho-Juan O 2009 *PhD Thesis* unpublished
[25] Katsikini M, Paloura E C and Moustakas T D 1998 *J. Appl. Phys.* **83** 1437
[26] Blaha P, Schwarz K, Madsen G K H, Kvasnicka D and Luitz J 2001 *WIEN2k, An Augmented Plane Wave + Local Orbitals Program for Calculating Crystal Properties* K Schwarz, Techn. Universität Wien, Austria
[27] Monkhorst H J and Pack J D 1976 *Phys. Rev.* B **13** 5188
[28] Farges F 2005 *Phys. Rev.* B **71** 155109
[29] Yang X L, Chen Z T, Wang C D, Huang S, Fang H, Zhang G Y, Chen D L and Yang W S 2008 *J. Phys. D: Appl. Phys.* **41** 125002